energies

MDPI

Article

Electromechanical Analysis of the Medium Voltage Earthing Switch due to Short-Time and Peak Withstand Current Test

Maja Krčum [1], Marko Zubčić [1,*] and Tatijana Dlabač [2]

[1] Faculty of Maritime Studies, University of Split, Ul. Ruđera Boškovića 37, 21000 Split, Croatia
[2] Maritime Faculty, University of Montenegro, Dobrota 36, 85330 Kotor, Montenegro
* Correspondence: mzubcic@pfst.hr

Received: 26 July 2019; Accepted: 16 August 2019; Published: 20 August 2019

Abstract: The chosen electrical equipment, i.e., the earthing switch has its application in marine switchgear. In this paper, the reduction of dimensions is considered with the purpose of making it more energy efficient in terms of onboard application. This test validates that the earthing switch as an electromechanical device is capable of withstanding electrodynamic forces. Two approaches are applied and compared. Both approaches are based on a simplified three-dimensional (3D) model of the earthing switch. The first approach is analytical: the electrodynamic forces are calculated with the assumption that currents flow in concentrated lines. Maximum static stress is compared to the yield point of the earthing knife material. The second approach applies the finite element method in the time domain. The results show that the rectangular cross-section can withstand the electrodynamic forces produced by the given currents. Simple cost analysis shows how much material is saved by changing the design from standard earthing knifes with C channel profile to the rectangular profile. Material savings make this study interesting for marine switchgear application. The paper shows qualitative influence of the obtained results on the Energy Efficiency Design Index of the ships.

Keywords: finite element method; mechanical stress; medium voltage earthing switch; type test; energy efficiency design index

1. Introduction

The medium-voltage (MV) earthing switch for indoor use is normally a part of MV switchgear. All switching apparatus of the MV switchgear are subjected to type testing. The test of interest in this paper is the short-time withstand current and peak withstand current test for the MV earthing switch that is described in [1]. The test proves the capability of the earthing switch to withstand mechanical stress due to electrodynamic forces that are caused by three-phase short-circuit currents. These forces are also called Lorentz forces. The rated short-time withstand current is chosen by the manufacturer from the R 10 series and the peak value is obtained by multiplying short-time withstand current value by 2.5 for rated frequency of 50 Hz. R10 series or Renard series is system of preferred numbers, which consists of the following numbers: 10, 12.5, 16, 20, 25, 31.5, 40, 50, 63, 80, and 100. The rated short-time withstand current is chosen by taking the number from Renard series and multiplying it with 1000. For the purpose of the analysis, the rated short-time withstand current of 16 kA/3 s and the peak withstand current value of 40 kA are chosen. There are many manufacturers of MV earthing switches that are present on the market, with each of them having their own design. One feature of the design is the cross-section profile and a number of earthing knifes per phase [2,3]. This paper discusses an MV earthing switch of RGB 38-25 type, manufactured by KONČAR-Electrical Equipment Inc. [4]. In Figure 1 the current path of the earthing switch RGB 38-25 is shown. This

earthing switch has two earthing knifes per phase and the cross-section of the knife is a C channel profile. The manufacturers always strive for better efficiency and performances of the product along with the cost of manufacturing reduction, material savings, and time-production saving. The C channel profile provides a bigger moment of inertia than the rectangular profile [5]. However, the elimination of the braces, i.e., substituting a C profile with a rectangular one, leads to material and time-production savings.

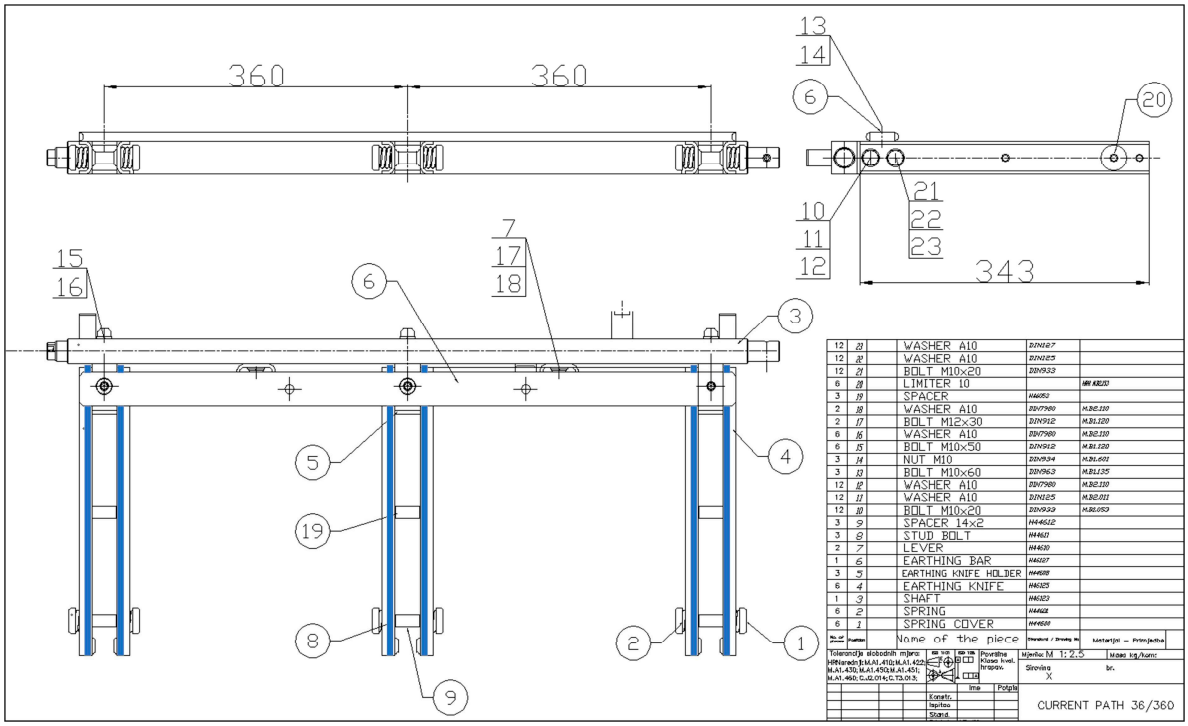

Figure 1. Medium-voltage (MV) earthing switch type RGB 38-25 detail drawings; for the purpose of comparison the blue color is showing the alternative design (copper knifer without braces).

The marine application is another aspect of the MV earthing switch redesign [6]. The need for electrical power increases the use of MV switchgear equipment on board [7]. Every MV cubical has an earthing switch. It is desirable that this system, along with other incidental systems, is smaller in size and weight. The reduction of the onboard equipment weight results in the decrease in fuel oil consumption [8]. Furthermore, this has a positive effect on air pollution that is caused by ships. The contribution of redesign can be expressed through the Energy Efficiency Design Index (EEDI) of the ship. The EEDI is a non-prescriptive, performance-based mechanism that leaves the choice of technologies to use in a specific ship design to the industry [9]. This paper examines the mechanical stress on earthing knifes with the rectangular cross-section during short-time withstand and peak withstand current test. The C channel profile reduces mechanical stress, but, from the cost analysis point of view, it increases the copper weight and the surface area of the earthing knife. One of the production line points of the RGB 38-25 is the silver coating of the copper earthing knifes. Silver coating is an expensive process, whose cost is proportional to the surface area of the copper. The mechanical stress on earthing knifes is calculated using the electrodynamic force calculation and mechanical static stress calculation for busbars of the rectangular cross-section [10]. The results that were analytically obtained are compared with the results from the finite element method (FEM) calculation. FEM calculation in the time domain, along with the simplified three-dimensional (3D) model of RGB 38-25 is made in "COMSOL Multiphysics" platform (5.2, COMSOL, Inc, Stockholm, Sweden) [11]. The simple cost analysis is conducted to highlight the influence of braces on earthing knife weight and surface. In addition to the relevant reference publications, our research also included simulation modelling that was supported by COMSOL Multiphysics software. This paper only contains the end results due to

limited space. The contribution of this study lies in the proposal that the earthing switch should be minimized, i.e., further reduced in size, in order to be embedded into modern engine room switchboard.

This paper proposes the improvement of the existing earthing switch. The accent is on the theoretical aspect of improvement.

2. Simulation Currents

Even though RGB 38-25 is certified for the 40 kA peak withstand current and 16 kA short-time withstand current of 3 s duration, the norm IEC 62271-1 (IEC—International Electrotechnical Commission) prescribes tolerances for current values. The peak current (for a three-phase circuit, the highest value in one of the outer phases) shall not be less than the rated peak withstands current. It shall not exceed it by more than 5% without the consent of the manufacturer. The average of the rms values of the AC component of the test currents shall not be less than the rated value [12]. The simulation currents that were used in this investigation comply with IEC norm prescribed tolerances. The three-phase resistive-inductive (RL) circuit is used to simulate the currents. The equations for currents in each phase are given, as follows [13]:

$$i_{L1} = \frac{U_m}{Z}\left(\sin(\omega t + \alpha - \gamma) - \sin(\alpha - \gamma)e^{-\frac{t}{\tau}}\right) \quad (1)$$

$$i_{L2} = \frac{U_m}{Z}\left(\sin\left(\omega t + \alpha - \gamma - \frac{2\pi}{3}\right) - \sin\left(\alpha - \gamma - \frac{2\pi}{3}\right)e^{-\frac{t}{\tau}}\right) \quad (2)$$

$$i_{L3} = \frac{U_m}{Z}\left(\sin\left(\omega t + \alpha - \gamma - \frac{4\pi}{3}\right) - \sin\left(\alpha - \gamma - \frac{4\pi}{3}\right)e^{-\frac{t}{\tau}}\right) \quad (3)$$

where U_m is maximum phase voltage, Z is impedance of RL circuit, R resistance, L inductance, $\omega = 2\pi f$ angular frequency, f frequency of the electrical grid, which is, in this discussion 50 Hz, γ phase shift, τ time constant of RL circuit, α closing angle, which defines the voltage value at the moment of short circuit occurrence. The equations are implemented in MATLAB (9.1, R2016b, The MathWorks, Inc, Natick, MA, USA). The basis for parameters of Equations (1)–(3) is the test report of the earthing switch RGB 38-25. This test report states if the earthing switch passed or did not passed the short-time withstand current and peak withstand current test. In the test report, the test currents are stated (16 kA/3 s and 40 kA peak value) and the time-current diagram of each phase is shown. To match test currents and time-current diagram curves the following parameters for Equations (1)–(3) are chosen:

$$(U_m,\ \tau, R, L, \alpha) = \left(\frac{10\sqrt{2}}{\sqrt{3}}\ \text{kV},\ 60.3\ \text{ms},\ 0.01876\ \Omega, 1.129\ \text{mH},\ 172.26^\circ\right) \quad (4)$$

Graphic representation of Equations (1)–(3), along with (4), as plotted in MATLAB, is shown in Figure 2. Table 1 presents peak values and short-time withstand current (r.m.s.) values.

Table 1. Peak current and short-time r.m.s. current for each phase.

Phase	Peak Current Value (kA)	Short-Time Current Value (r.m.s.) (kA)
L1	42.33	16.25
L2	34.66	16.25
L3	30.82	16.25

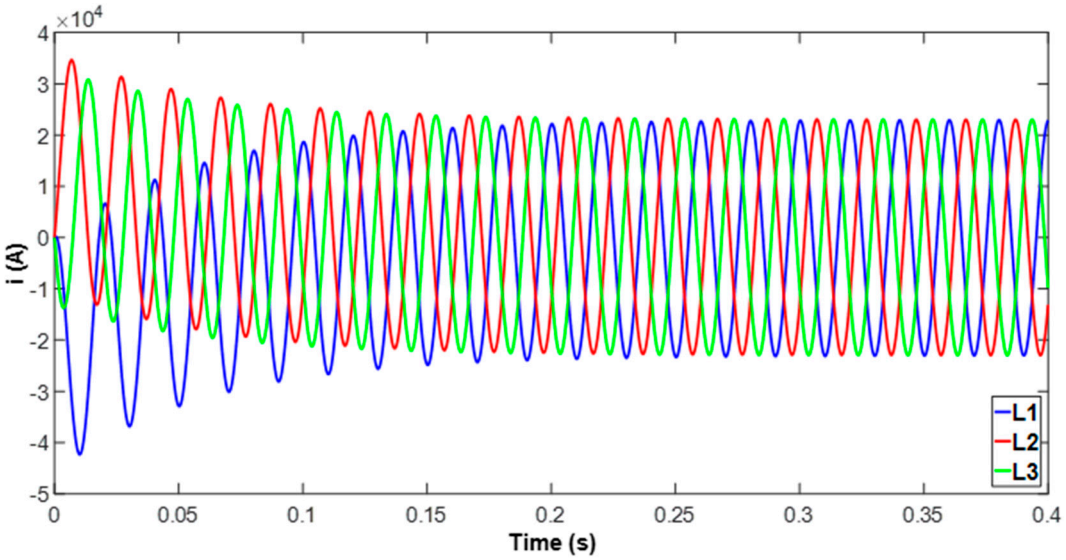

Figure 2. Simulation current for each phase.

3. Electrodynamic Forces

The simple approach for electrodynamics force calculation implies that all of the current paths are straight lines on which the current is concentrated. As this earthing switch has two busbars per phase, the input current is considered to be divided equally between the earthing knifes $i_{11} = i_{12}$, etc. Only the x component of the electrodynamic force is considered. Figure 3 shows the top view of the earthing knife along with current lines, current designation for each phase, and earthing knife designations (L11–L32). Electrodynamic forces on the earthing knife are calculated by using the equations for parallel finite length conductors and equations for finite length conductors at right angle. Two conductors at right angle can be connected or separated (see Figure 4b). Electrodynamic force on earthing knife L11 is produced by parallel conductors [14]:

$$\begin{aligned} F_{p11} = \left(2{\cdot}10^{-7}\right) i_{11}\Big[& k_D(d,b,c) i_{12} k_{fl}(l,d) \\ & + k_D(a,b,c) i_{21} k_{fl}(l,a) \\ & + k_D(a+d,b,c) i_{22} k_{fl}(l,a+d) \\ & + k_D(2a,b,c) i_{31} k_{fl}(l,2a) \\ & + k_D(2a+d,b,c) i_{32} k_{fl}(l,2a+d)\Big] \end{aligned} \tag{5}$$

In Table 2, the geometrical design parameters are shown.

Table 2. Design input parameters.

Design Input	Value
Number of busbars per phase	2
Length of a busbar knife	343 mm
Height of busbar knife	40 mm
Thickness of a busbar knife (c)	4 mm
Distance between the knifes of the same phase (d)	34 mm
Center-line distance between phases (a)	360 mm
Short-link busbar dimensions	780 mm × 40 mm
C channel dimensions	Figure 5a
Rectangular knife dimensions	Figure 5b
Segment length s_1, s_3, s_5 (Figure 3)	34 mm
Segment length s_2, s_4 (Figure 3)	326 mm
Length of a current line in the knife (l) (Figure 3)	315 mm

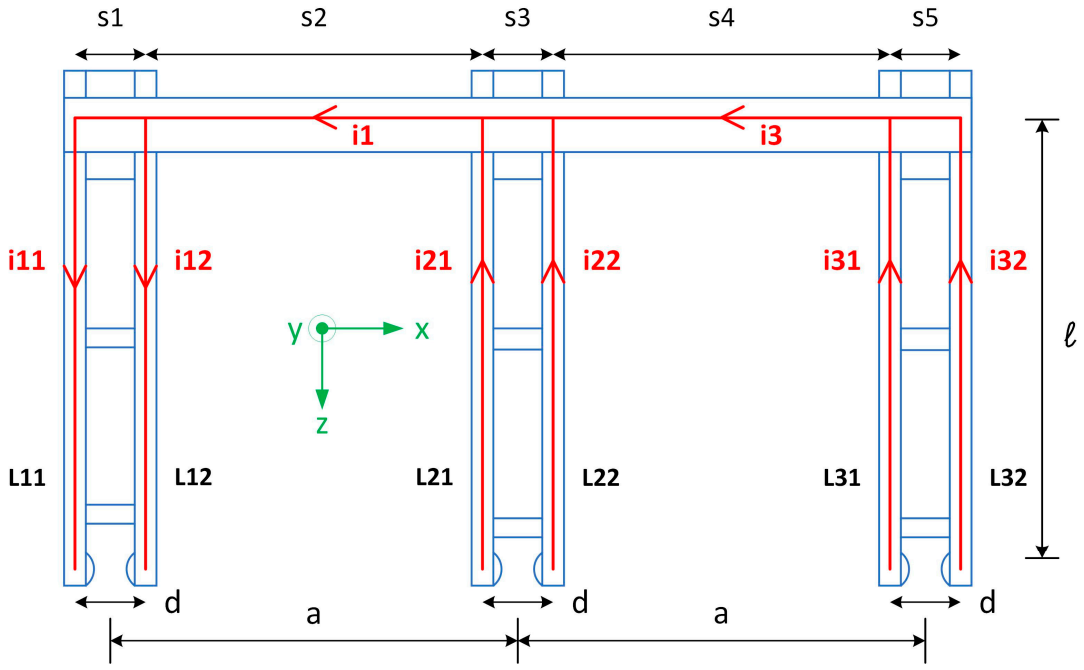

Figure 3. Top view of the earthing switch—red lines represent current lines, s1–s5 represent segments for force calculation on conductors at right angle, L11–L32 represent designations of each earthing knife.

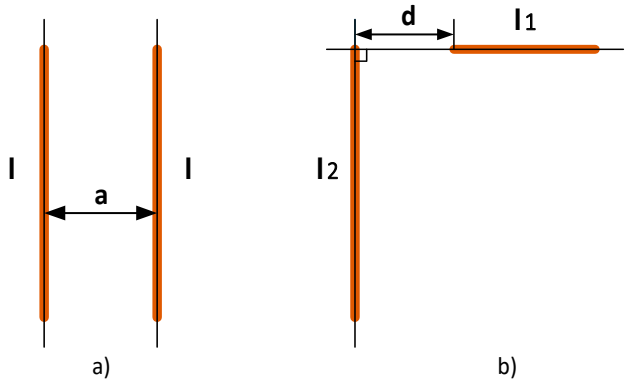

Figure 4. Conductors of finite length: (**a**) parallel conductors of the same length separated by distance a, (**b**) conductors of different length at the right angle and separated by distance d.

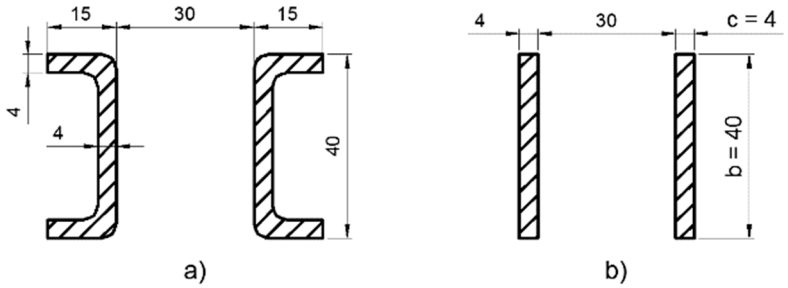

Figure 5. Cross-section of the earthing knife of one phase: (**a**) type RGB 38-25, (**b**) subject of this paper; (dimensions are in mm).

Where i_{11} is the current through knife L11, i_{11} is the current through knife L12. k_D is Dwight's coefficient [15], which is a function of distance between two busbars of the rectangular cross-section

and the dimensions of the busbar (see Figure 5b). k_{fl} is a coefficient that takes into account the finite length of busbars and it is a function of the distance between busbars and their length [14]:

$$k_{fl}(l,d) = \sqrt{\left(\frac{l}{d}\right)^2 + 1} - 1 \tag{6}$$

where l is the length of a busbar and d stands for the distance between conductors.

Electrodynamic force on earthing knife L11 produced by current i_{11} flowing through segment s_1, which is conductor at right angle and connected to L11 [16]:

$$F_{s1\_11} = 10^{-7} i_{11} i_{11} k_{cs}(s_1, l, b, c) \tag{7}$$

where k_{cs} is the coefficient which is a function of s_1 segment length, earthing knife L11 length l and busbars dimensions b and c [16]:

$$k_{cs}(s_1, l, b, c) = \ln\left(\frac{l}{g_{11}} \frac{s_1 + \sqrt{s_1^2 + g_{11}^2}}{s_1 + \sqrt{s_1^2 + l^2}}\right) \tag{8}$$

where $g_{11} = 0.2235(c + b)$ is the coefficient for the rectangular cross-section busbar [16].

Electrodynamic force on earthing knife L11 produced by current i_1 flowing through segment s_2, which is conductor at right angle and separated by distance s_1:

$$F_{s2\_11} = 10^{-7} i_1 i_{11} k_{ds}(s_2, l, s_1) \tag{9}$$

where k_{ds} is the coefficient that is a function of s_2 segment length, earthing knife L11 length l, and separation s_1:

$$k_{ds}(s_2, l, s_1) = \ln\left(\frac{s_1 + s_2}{s_1} \frac{s_1 + \sqrt{s_1^2 + l^2}}{(s_1 + s_2) + \sqrt{(s_1 + s_2)^2 + l^2}}\right) \tag{10}$$

Electrodynamic forces on knife L11 that are caused by currents flowing through segments s_3, s_4, and s_5 are analogously calculated. Total force on earthing knife L11 in x direction [15]:

$$F_{L11} = F_{p11} - F_{s1\_11} - F_{s2\_11} + F_{s3\_11} + F_{s4\_11} + F_{s5\_11} \tag{11}$$

The total forces on earthing knifes L12–L32 are calculated analogously. Figures 6–8 show electrodynamic forces on earthing knifes L11–L31 in x direction.

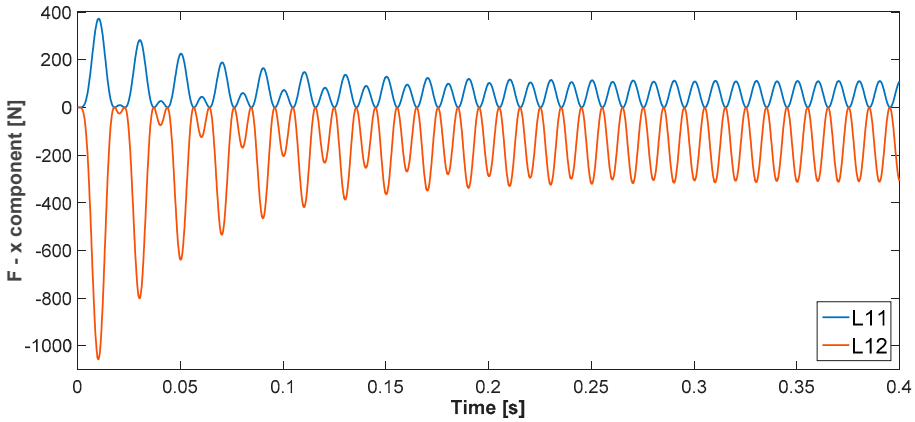

Figure 6. Electrodynamic forces on earthing knifes L11 and L12.

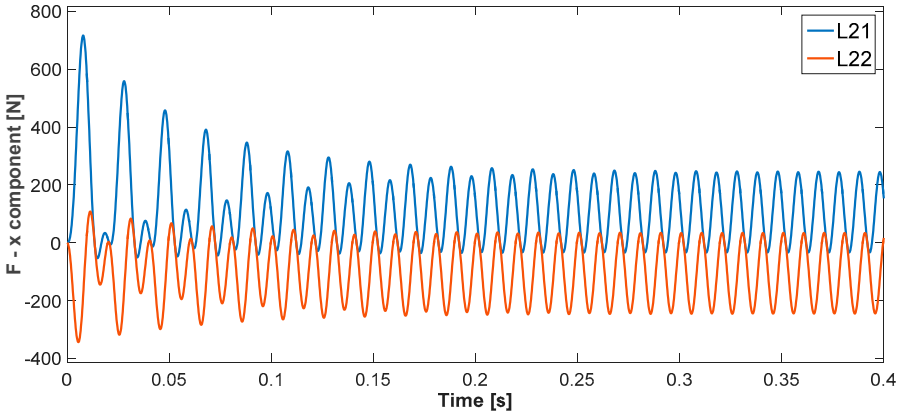

Figure 7. Electrodynamic forces on earthing knifes L21 and L22.

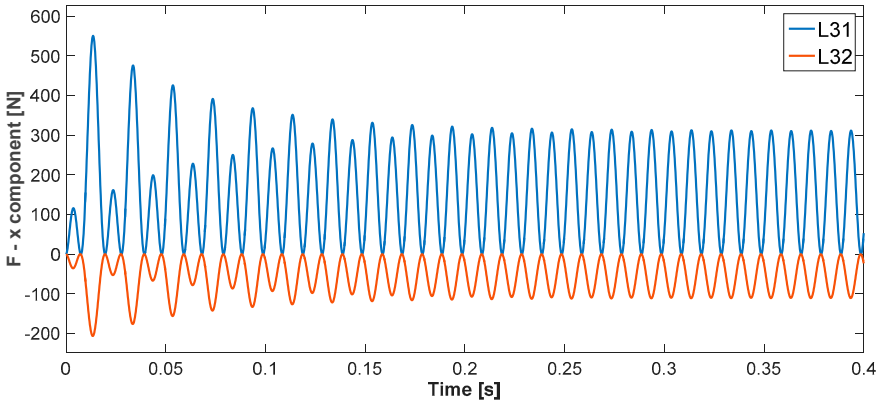

Figure 8. Electrodynamic forces on earthing knifes L31 and L32.

In Table 3, the absolute maximum value of the force for each earthing knife in transient and in stationary state is presented. The results in Table 3 show that knife L12 is exposed to maximum force of 1056.90 N. This force will be the input force for stress calculation.

Table 3. Maximum forces on knifes in transient and in stationary state.

Knife	Transient: |*Fmax*| (N)	Stationary: |*Fmax*| (N)
L11	372.59	110.88
L12	1056.90	312.54
L21	716.97	245.93
L22	344.06	245.42
L31	550.36	311.69
L32	206.08	110.55

4. Stress Calculation

In this study, the earthing knife is a beam with three spans and uniformly distributed load (see Figure 9).

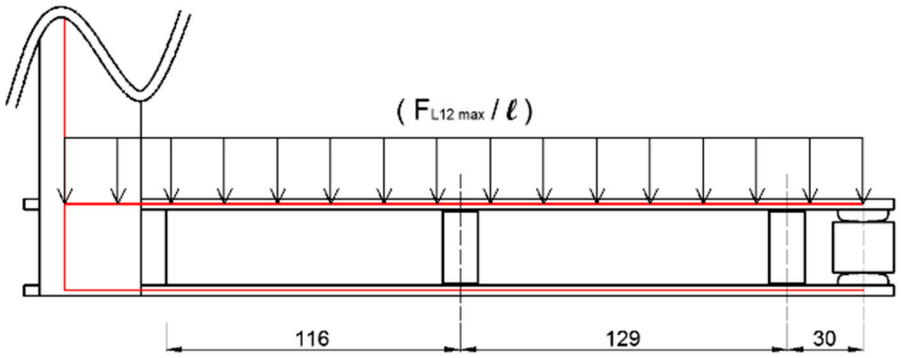

Figure 9. Phase L1—uniformly distributed load on knife L12.

The spacers are fixed supports. The first span of length $l_{span1} = 0.116$ m represents the part of the beam that is fixed on both ends. The second span of length $l_{span2} = 0.129$ m also represents the part of the beam that is fixed on both ends. The third span of length $l_{span3} = 0.03$ m represents the part of the beam that is fixed at one end and is freely supported at the other end. The bending stress of the beam fixed at both ends is calculated while using equation [17]:

$$\sigma = \frac{M_{max}}{W} = \frac{F_{L12\_max} \cdot l_{span}}{12\frac{bc^2}{6}} \tag{12}$$

where W is section modulus of the beam, M_{max} is maximum bending moment, F_{L12_max} is the maximum force on L12 earthing knife. The bending stress of the beam fixed at one end, and freely supported at the other end, is being calculated by equation [17]:

$$\sigma = \frac{M_{max}}{W} = \frac{F_{L12\_max} \cdot l_{span}}{8\frac{bc^2}{6}} \tag{13}$$

Table 4 presents the stress values for each span. The conductor should withstand the electrodynamics forces when:

$$\sigma \leq qR_{p0,2} \tag{14}$$

where $R_{p0,2}$ is the stress corresponding to the yield point and q is the factor that describes the increase in the permitted stress of the conductor due to its plastic behavior at places outside of its supports. The shape of the conductor should be taken into account [18]. For the rectangular cross-section the value of q is 1.5.

Table 4. Stress values for each span.

Span	l_{span} (m)	M_{MAX} (Nm)	σ (N/mm^2)
1	0.116	10.21	95.70
2	0.129	11.35	106.42
3	0.030	3.96	37.12

The copper that is used for earthing knifes is electrolytic tough-pitch half-hard copper, whose mechanical properties are described in [19]. Yield stress for this copper is $R_{p0,2} = 176.52$ N/mm^2 (material chosen by the manufacturer). Therefore, the condition (14) is satisfied for every span in Table 4.

5. Finite Element Method

5.1. 3D Model

The MV earthing switch RGB 38-25 is a complex mechanical object. It consists of six earthing knifes, three isolators, mechanical joint elements, the shaft on which the earthing knifes along with copper shortening link is mounted, mechanical linkage that rotates the shaft due to operator manipulation, springs for fast closing operation, metal base whose purpose is to fix the earthing switch to a metal side of a MV switchgear cable compartment.

The simplified 3D model is made and investigated in "COMSOL Multiphysics" platform because of the complexity of the earthing switch geometry. Only the active part of the earthing switch is modeled. Active parts are those parts that conduct electrical current. The springs, insulators, bolts, washers, metal base, and metal linkage are neglected. Simplification comes from the consideration that forces only act in x direction in the active part of the earthing switch. Forces acting in y direction are negligible (coordinates are shown in Figure 3). Regarding forces in x direction, it is true that insulators suffer also some stress during test but the insulators are mechanically supported with the busbars that they are connected to in closed position. Disregarding the insulators, big reduction in the number of the FEM elements, and thus the computation time is achieved. The rotating bar on which active part is mounted to is disregarded, because of no force in y direction. It means that there is no momentum acting on earthing switch that could rotate during testing. The induced currents in the rotating bar are neglected. Accordingly, there is no electrodynamical force interaction with the active part. From all of this follows that rotating bar is completely stationary during the test. A disregarded rotating bar is replaced in the model with mechanical boundary condition $u = 0$. The springs for the contacts which can also be seen on Figure 1 are disregarded. Springs produce large number of FEM elements because of their complexity and size, thus increasing the computation time. In the model the springs are replaced with a force vector acting in the same direction as the spring. The magnitude of the force vector is taken from the technical documentation which stated spring dimensions and the elongation-force graph.

The 3D model is surrounded by air. Figure 10 shows the simplified model of the RGB 38-25 earthing switch.

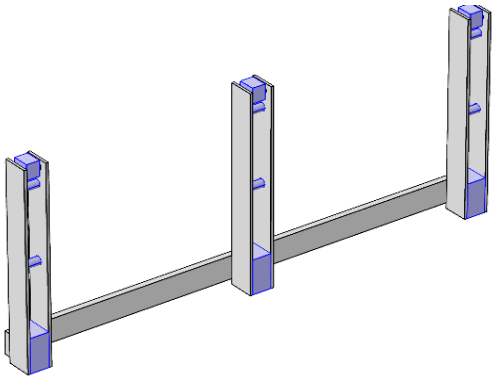

Figure 10. Simplified 3D model in COMSOL Multiphysics (5.2, COMSOL, Inc, Stockholm, Sweden); blue colour—domains on which boundary condition $u = 0$ is imposed.

Two modules are used in COMSOL to apply the short-time withstand and peak withstand current defined by the manufacturer and to calculate the mechanical stress. The first is the AC/DC module, which consists of several interfaces. In the modeling of the desired current wave-form and calculating of electromagnetic quasi-stationary field, the following interfaces are used: electrical circuit, electrical currents, and magnetic field interface. The second one is the Structural Mechanics module, which also consists of several interfaces. The interface that is used to calculate the mechanical stresses is a solid

mechanics interface. When looking at the used modules, this problem can be referred to as the coupled electro-mechanic problem.

5.2. Solid Mechanics Boundary Condition

Under the assumption that the Lorentz forces can be neglected in the y and z directions, the displacement boundary condition $u = 0$ can be imposed on the surfaces that are shown in Figure 10. This boundary condition substitutes the rotating shaft on which the active parts are mounted.

6. FEM Results

Electrodynamic force wave forms on the earthing knifes that were obtained by FEM calculation in COMSOL are shown in Figures 11–13.

Tables 5 and 6 present the comparison of the electrodynamic forces that were obtained by analytical and FEM calculations. In Table 5, the comparison is given for the transient state. In Table 6, the comparison is given for the stationary state. The difference between the analytical and FEM results is calculated by the following equation:

$$Difference(\%) = \frac{FEM - Analytical}{Analytical} \times 100 \quad (15)$$

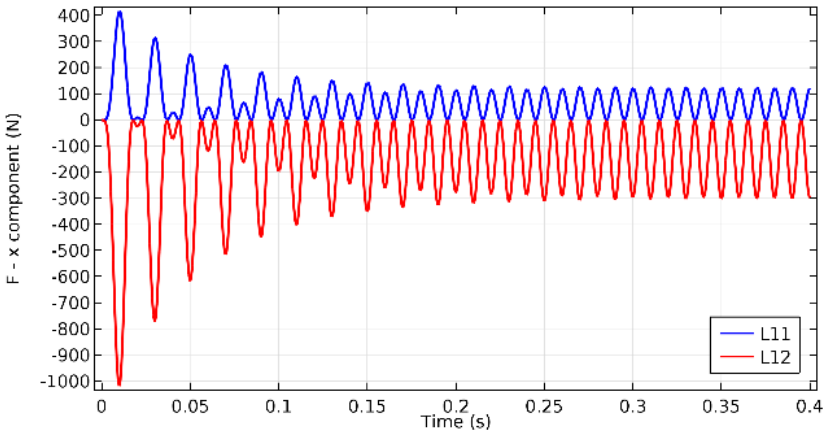

Figure 11. Electrodynamic forces on earthing knifes L11 and L12 obtained by finite element method (FEM) calculation.

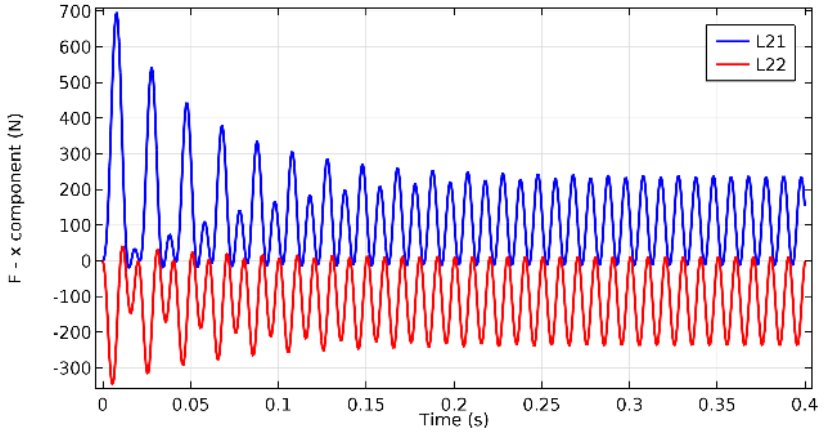

Figure 12. Electrodynamic forces on earthing knifes L21 and L22 obtained by FEM calculation.

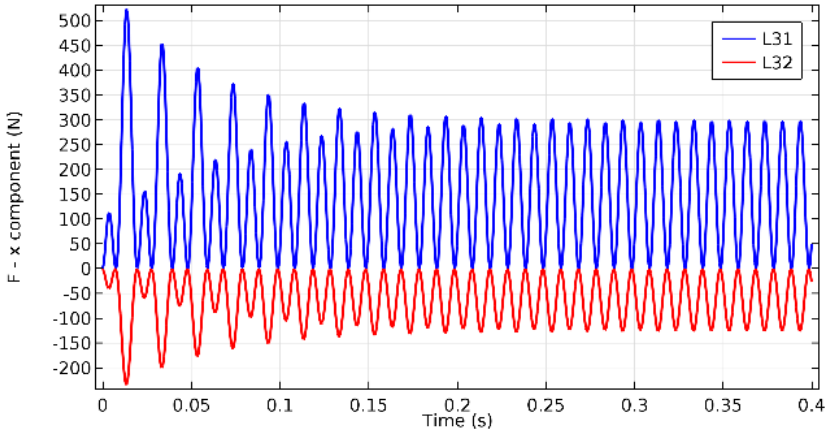

Figure 13. Electrodynamic forces on earthing knifes L31 and L32 obtained by FEM calculation.

Table 5. Comparison of electrodynamical forces for transient state.

Knife	|Analytical| (N)	Transient |FEM| (N)	Difference (%)
L11	372.59	417.77	12.13
L12	1056.90	1019.10	−3.58
L21	716.97	697.20	−2.75
L22	344.06	345.88	0.53
L31	550.36	523.46	−4.88
L32	206.08	234.02	13.55

Table 6. Comparison of electrodynamical forces for stationary state.

Knife	|Analytical| (N)	Stationary |FEM| (N)	Difference (%)
L11	110.88	123.96	11.80
L12	312.54	300.15	−3.96
L21	245.93	238.57	−2.99
L22	245.42	236.96	−3.44
L31	311.69	297.80	−4.45
L32	110.55	125.14	13.20

In COMOSL, the Von Mises stress is calculated [20,21]. The Von Mises stress distribution over the earthing switch in MPa and the point of maximum Von Mises stress (red marking) is shown in Figure 14. The distribution is presented for t = 0.01 s. In that moment, the maximum force occurs on knife L11. Figure 15 highlights the point where maximum stress occurs.

Maximum Von Mises stress occurs in the point where knife L12 and upper spacer (looking from the bottom of the earthing switch) are in contact. The value of maximum stress is:

$$\sigma_{VMmax} = 130.03 \text{ MPa} \tag{16}$$

This value satisfies the Equation (14).

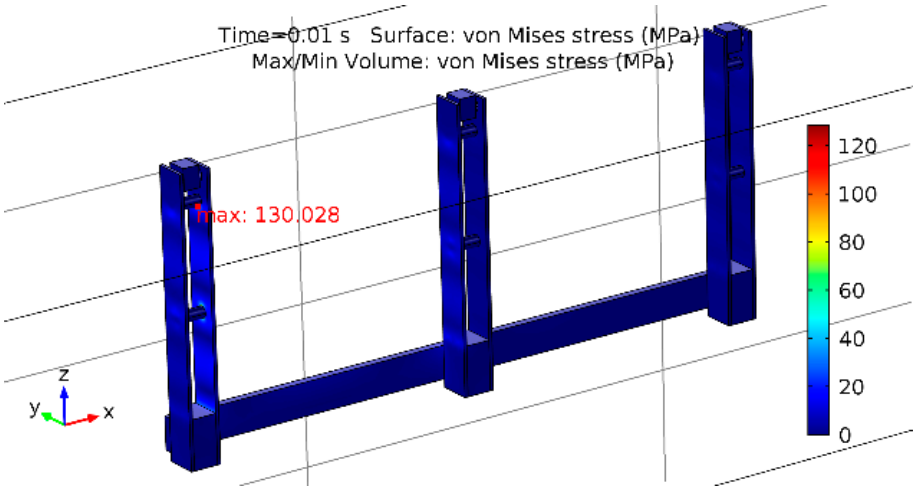

Figure 14. Von Mises stress distribution over the earthing switch.

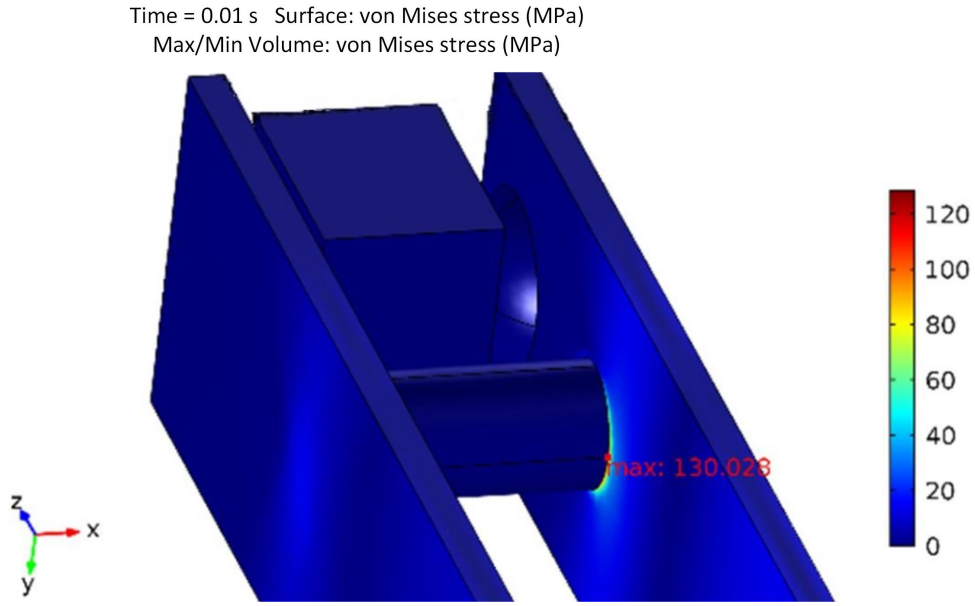

Figure 15. Phase L1—knife L12—the point of maximum Von Mises stress-red marking.

7. Cost Analysis

By eliminating the braces of the earthing knife, the weight and surface area of the earthing knife is reduced. Thus, the cost of material (copper) and the cost of silver coating are reduced. The mass and surface area of one earthing knife can be expressed, as follows:

$$m' = \rho V' = \rho(bc + 2cBL) \tag{17}$$

$$S' = 2b + 2c + 4BL \tag{18}$$

where m' is mass per unit length, V' volume per unit length, S' surface per unit length, ρ is mass density of material, b is the height of the rectangular cross-section, c is the width, and BL is the brace length. In this research, the brace length is $BL = 11$ mm (see Figure 5a).

The calculation of the mass per unit length ratio for earthing knife with and without braces gives:

$$\frac{m'_{with\ braces}}{m'_{without\ braces}} = 1.55 \tag{19}$$

For the surface area ratio:

$$\frac{S'_{with\ braces}}{S'_{without\ braces}} = 1.50 \tag{20}$$

The mass reduction is important from the manufacturer point of view. If the function of the product is preserved less mass means lower manufacturing cost. From the application point of view the mass reduction is important in transportation industry. In this paper, the accent is on the marine industry. Mass reduction achieved by the alternative design means the mass reduction of onboard medium voltage switchboard. This further leads to lower fuel consumption that has economic and environmental impact.

8. Energy Efficiency Design Index

Marine traffic contributes to Greenhouse Gas (GHG) emissions. Globally, marine traffic is considered to be a highly energy efficient mode of transportation [22]. Figure 16 shows the marine traffic GHG emission on global scale. Nevertheless, this ratio can be different when one investigates GHG emission on a regional scale.

Figure 16. CO_2 emissions for different types of transport, source [23].

Figure 17 shows the shares of different traffic mode in GHG emissions for European Union (EU). International Maritime Organization (IMO) formulated the Energy Efficiency Design Index (EEDI) with a purpose to reduce CO_2 emission from shipping. Since 1st January 2013, every ship must have the International Energy Efficiency Certificate (IEEC). One of the conditions, which is relevant to this study, is compliance with EEDI requirements. EEDI is a technical measure that promotes the use of energy efficient equipment on ships [25]. Factors that define EEDI are ship power system CO_2 emission, deadweight tonnage (DWT), and speed V (in knots). Simplified formula for EEDI taken from [26,27] is:

$$EEDI = \frac{CO_2\ emission}{Transport\ work} = \frac{ME\ emissions}{Transport\ work} + \frac{AE\ emissions}{Transport\ work} \frac{Shaftgenerators/motors\ emissions}{Transport\ work} - \frac{Efficiency\ techonologies}{Transport\ work} \tag{21}$$

where ME is short for Main Engines, AE is short for Auxiliary Engines, Transport work is the product of DWT and the speed of the ship. Complete formula can be found in [28,29]. The MV earthing switch is one of the many components on the ship that optimization can contribute to overall EEDI reduction. The contribution comes from the Efficiency technologies (ET) term in the Equation (21):

$$ET = \sum_{i=1}^{neff} f_{eff(i)} \cdot P_{eff(i)} \cdot C_{FME} \cdot SFC_{ME} \tag{22}$$

where $f_{eff(i)}$ is availability factor of individual efficiency technologies, $P_{eff(i)}$ is main engine power reduction due to individual technologies for mechanical energy efficiency, C_{FME} is main engine composite fuel factor, and SFC_{ME} is main engine specific fuel consumption.

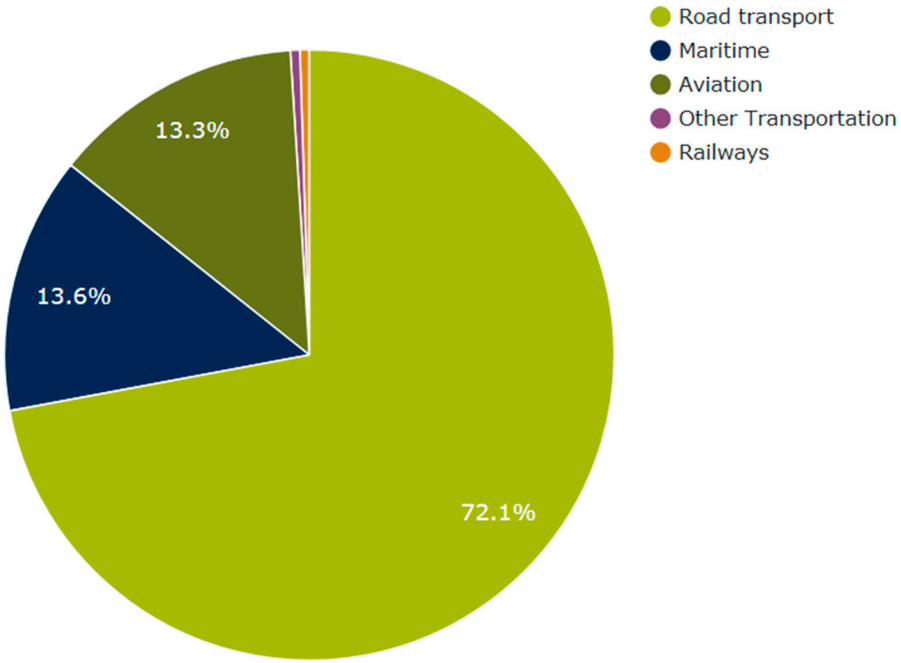

Figure 17. Share of different transportation modes in Greenhouse Gas (GHG) emissions in the European Union (EU), source [24].

The mass reduction of the earthing switch, thus also the mass reduction of medium voltage electrical equipment on bord is:

$$V = (c{\cdot}b + 2{\cdot}c{\cdot}BL){\cdot}l = 8.5064{\cdot}10^{-5}\ \mathrm{m}^3 \tag{23}$$

$$m_{ES} = 6{\cdot}m_{knife} = 6{\cdot}\rho V = 4.56\ \mathrm{kg} \tag{24}$$

$$V' = (c{\cdot}b){\cdot}l = 5.4880{\cdot}10^{-5}\ \mathrm{m}^3 \tag{25}$$

$$m'_{ES} = 6{\cdot}m'_{knife} = 6{\cdot}\rho V' = 2.94\ \mathrm{kg} \tag{26}$$

$$\Delta m = m_{ES} - m'_{ES} = 1.62\ \mathrm{kg} \tag{27}$$

where V is the volume of the one knife with braces, b is height of the knife, c is the width of the knife, BL is the brace length, l is the length of the knife, m_{knife} is the mass of one knife with braces, m_{ES} is the mass of the six knifes with braces, V' is the volume of the one knife without braces, m'_{knife} is the mass of one knife without braces, m'_{ES} is the mass of the six knifes without braces, ρ is copper density, and Δm is mass reduction due to earthing knifef braces elimination.

The ship power substation can have anywhere between 3 to 40 medium voltage switchgear feeders. This depends on the installed power of the ship. Every feeder contains a earthing switch (Figure 18). This gives the mass reduction of a onboard substation:

$$\Delta m_{substation} = n{\cdot}\Delta m \tag{28}$$

where $\Delta m_{substation}$ is mass reduction of the substation due to the mass reduction of the earthing switch and n is the number of feeders of the substation. For $n = 5$, the mass reduction is $\Delta m_{substation} = 8.1$ kg and for $n = 40$, $\Delta m_{substation} = 64.8$ kg.

Even though the overall mass reduction of one earthing switch is negligible when compared to merchant ship or a cruise ship, the idea is to encourage the manufacturers of electrical equipment to reduce the mass and the dimensions of electrical power system components. In this way, the electrical part of the ship can contribute to the energy efficiency of the ship.

Mass reduction of onboard electrical equipment results in total ship resistance decrease, which leads to lower power demand from the main engine to maintain constant speed, thus the overall effect is lower fuel consumption.

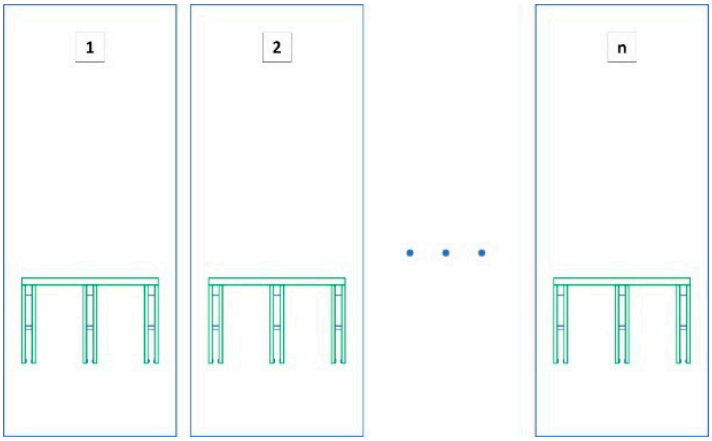

Figure 18. Medium voltage switchgear feeders containing earthing switches.

9. Conclusions

The investigation is made with the aid of a simplified model while using an analytical approach for electrodynamic force and the static stress calculation along with FEM approach in the "COMSOL Multiphysics" platform. The results regarding electrodynamic forces in transient and stationary states are in good compliance with all knifes, except for L11 and L32. These knifes are the outermost knifes.

Even though the nature of the calculated stresses is different, the analytical approach gives static stress and an FEM analysis gives the information about Von Mises stress. The overall results show that maximum stresses are below the yield point of the used material. Therefore, the produced results indicate that the earthing switch without braces can withstand electro dynamical forces that are produced by simulation currents during the type test. In addition, it is shown that brace elimination provides significant cost saving in material and silver coating.

The Energy Efficiency Design Index is introduced as a measure of overall ship efficiency regarding CO_2 production. It is qualitatively shown how mass reduction of the earthing switch can affect the EEDI.

The future research will incorporate the geometry design investigations regarding mass and size reduction, thus contributing to CO_2 reduction from ships due to electrical equipment component. The next step is to investigate the electrodynamic forces for the reduced distance between earthing knifes of the same size. By reducing the distance between them, the mechanical element, which holds the earthing knifes, will also be reduced in size and mass.

Author Contributions: M.K. and T.D. contributed to paper writing and whole revision process. M.Z. built the simulation model and analyzed the data. The final manuscript has been read and approved by all named authors.

Funding: This research received no external funding.

Acknowledgments: Authors would like to thank KONČAR-Electrical Equipment Inc. for providing a detailed insight into their earthing switch RGB 38-25 design.

Conflicts of Interest: The authors declare no conflict of interest.

References

1. International Electrotechnical Commission. *IEC 62271-102:2012. High-Voltage Switchgear and Controlgear—Part 102: Alternating Current Disconnectors and Earthing Switches*; International Electrotechnical Commission: Geneva, Switzerland.

2. ABB. OJWN Earthing Switches with Fault Making Capacity. Available online: http://new.abb.com/medium-voltage/apparatus/isolators-switches-disconnectors/indoor-switches/earthing-switches/iec-indoor-earthing-switch-ojwn (accessed on 6 April 2018).
3. SIEMENS. Medium Voltage Indoor Devices. Available online: https://w3.siemens.nl/powerdistribution/nl/nl/mv/medium-voltage-indoor-devices/Pages/medium-voltage-indoor-devices.aspx (accessed on 6 April 2018).
4. KONČAR-Electrical Equipment. MV Earthing Switches. Available online: http://www.koncareu.hr (accessed on 15 December 2017).
5. Copper Development Association. Copper for Busbars-Guidance for Design and Installation. Available online: http://copperalliance.org.uk/docs/librariesprovider5/pub-22-copper-for-busbars/copper-for-busbars-all-sections.pdf?sfvrsn=2 (accessed on 6 April 2018).
6. TERASAKI. Medium Voltage, Arc-Proof, Air-Insulated, Metal-Clad Switchgear and Controlgear up to 12 kV. Available online: http://www.terasaki.co.jp/english/files/business/ship/HS21_P1116-Ec_web_16.12.02.pdf (accessed on 6 April 2018).
7. Khersonsky, Y.; Islam, M.; Peterson, K. Challenges of Connecting Shipboard Marine Systems to Medium Voltage Shoreside Electrical Power. *IEEE Trans. Ind. Appl.* **2007**, *43*, 838–844. [CrossRef]
8. Gorski, W.; Abramowicz-Gerigk, T.; Burciu, Z. The influence of ship operational parameters on fuel consumption. *Sci. J. Marit. Univ. Szczec.* **2013**, *108*, 49–54.
9. Energy Efficiency Measures. International Maritime Organization. Available online: http://www.imo.org/en/ourwork/environment/pollutionprevention/airpollution/pages/technical-and-operational-measures.aspx (accessed on 26 August 2018).
10. IEEE. *Guide for Design of Substation Rigid-Bus Structures*; IEEE: Piscataway, NJ, USA, 1987. [CrossRef]
11. COMSOL Multiphysics. User's Guide. Available online: http://people.ee.ethz.ch/~{}fieldcom/pps-comsol/documents/User%20Guide/COMSOLMultiphysicsUsersGuide.pdf (accessed on 6 April 2018).
12. International Electrotechnical Commission. *IEC 62271-1:2007. High-Voltage Switchgear and Controlgear—Part 1: Common Specifications*; International Electrotechnical Commission: Geneva, Switzerland.
13. Yusop, F.M.; Jamil, M.K.M.; Ishak, D.; Husaini, M.; Masri, S. Investigation of electromagnetic force during short-circuit test in three-phase busbar system. In Proceedings of the 2011 IEEE Colloquium on Humanities, Science and Engineering, Penang, Malaysia, 5–6 December 2011; pp. 340–344.
14. Schneider Electric. Electrodynamic Forces on Busbars in LV Systems. Available online: https://www.schneider-electric.com (accessed on 11 December 2017).
15. Kadkhodaei, G.; Sheshyekani, K.; Hamzeh, M.; Tavakoli, S.D. Multiphysics analysis of busbars with various arrangements under short-circuit condition. *IET Electr. Syst. Transp.* **2016**, *6*, 237–245. [CrossRef]
16. Knopf, R.; Cupsa, A. Electromagnetism, short-circuit forces and strains in elbow sections of phase-isolated, metal-enclosed generator busbars. *Eur. Trans. Electr. Power* **1994**, *4*, 537–546. [CrossRef]
17. ARIAN BAREZ COMPANY. ABB Switchgear Manual. Available online: http://www.arianbc.net (accessed on 14 December 2017).
18. International Electrotechnical Commission. *IEC 60865-1:2011. Short-Circuit Currents—Calculation of Effects—Part 1: Definitions and Calculation Methods*; International Electrotechnical Commission: Geneva, Switzerland, 2012.
19. Aurubis Finland Oy. Industrial Product, Specification. Available online: http://finland.aurubis.com (accessed on 14 December 2017).
20. Kadkhodaei, G.; Sheshyekani, K.; Hamzeh, M. Coupled electric–magnetic–thermal–mechanical modelling of busbars under short-circuit conditions. *IET Gener. Transm. Distrib.* **2016**, *10*, 955–963. [CrossRef]
21. Wang, S.; Wang, S.; Li, H.; Yuan, D.; Wang, S. Mechanical characteristics analysis of defective transformer windings under short-circuit fault using 3-D FEM. In Proceedings of the 2017 20th International Conference on Electrical Machines and System (ICEMS), Sydney, Australia, 11–14 August 2017. [CrossRef]
22. Winnes, H.; Styhre, L.; Fridell, E. Reducing GHG emissions from ships in port areas. *Res. Transp. Bus. Manag.* **2015**, *17*, 73–82. [CrossRef]
23. International Chamber of Shipping. Comparison of CO2 Emissions by Different Modes of Transport. Available online: http://www.ics-shipping.org/shipping-facts/environmental-performance/comparison-of-co2-emissions-by-different-modes-of-transport (accessed on 28 August 2018).

24. European Environment Agency. Greenhouse Gas Emission from Transport. Available online: https://www.eea.europa.eu/data-and-maps/indicators/transport-emissions-of-greenhouse-gases/transport-emissions-of-greenhouse-gases-10 (accessed on 19 August 2019).
25. Vladimir, N.; Ančić, I.; Šestan, A. Effect of ship size on EEDI requirements for large container ships. *J. Mar. Sci. Technol.* **2018**, *23*, 42–51. [CrossRef]
26. Zheng, J.; Hu, H.; Dai, L. How would EEDI influence Chinese shipbuilding industry? *Marit. Policy Manag.* **2013**, *40*, 495–510. [CrossRef]
27. The International Councile on Clean Transportation. The Energy Efficiency Design Index (EEDI) for New Ships. Available online: https://www.theicct.org/sites/default/files/publications/ICCTpolicyupdate15_EEDI_final.pdf (accessed on 25 August 2018).
28. Yuan, H.; Xiao, L.; Xu, M. Hull lines reliability-based optimisation design for minimum EEDI. *Shipbuild. Theory Pract. Nav. Archit. Mar. Eng. Ocean Eng.* **2018**, *69*, 17–33. [CrossRef]
29. Basic Principles of Ship Propulsion. MAN Diesel & Turbo. Available online: https://marine.mandieselturbo.com/docs/librariesprovider6/ppropelle-aftship/basic-principles-of-propulsion.pdf?sfvrsn=0 (accessed on 25 August 2018).